the National Science Foundation for its support of the NSF Northeast Regional NMR Facility (Grant CHE79-16210).

Registry No. $NMCpMo(CO)_2B$ (B = 1,3-dimethylallyl), 85565-44-2; $[NMCpMo(NO)(CO)B]PF_6$ (B = 1,3-dimethylallyl) (isomer 1), 85565-46-4; $[NMCpMo(NO)(CO)B]PF_6$ (B = 1,3-dimethylallyl) (isomer 2), 85646-37-3; $[NMCpMo(NO)(CO)B]PF_6$ (B = 1,3-dimethylallyl) (isomer 3), 85646-35-1; $[NMCpMo(NO)(CO)B]PF_6$ (B = 1,3-dimethylallyl) (isomer 4), 85646-39-5; $[NMCpMo(NO)(CO)B]BPh_4$ (B = 1,3-dimethylallyl) (isomer 1), 85699-63-4; $[NMCpMo(NO)(CO)B]BPh_4$ (B = 1,3-dimethylallyl) (isomer 2), 85646-40-8; NMCpMo(NO)(CO)B (B = (*R*)-2,2,3-trimethylhex-4-enal) (isomer 1), 85565-47-5; NMCpMo(NO)(CO)B (B = (*R*)-2,2,3-trimethylhex-4-enal) (isomer 2), 85646-41-9; $(+)_D$-NMCpMo(NO)(CO)B (B = 2,2,3-trimethylhex-4-enal) ((2,4-dinitrophenyl)hydrazone), 85565-48-6; $Mo(CO)_6$, 13939-06-5; $M(CO)_2(CH_3CN)_2(B)Br$ (B = 1,3-dimethyl)allyl), 85565-49-7; NMCpH, 69165-85-1; (+)-2,2,3-trimethylhex-4-enal, 85553-69-1; 2,2,3-trimethylhex-4-enal (*l*-menthyl hydrazide) (isomer 1), 85553-70-4; 2,2,3-trimethylhex-4-enol (*l*-menthyl hydrazide) (isomer 2), 85611-53-6; (+)-2,2,3-trimethylhex-4-enal ((2,4-dinitrophenyl)-hydrazone), 85553-71-5; 4-bromo-2-pentene, 1809-26-3; 1-pyrrolidino-2-methylpropene, 2403-57-8; *l*-menthyl hydrazide, 85553-68-0.

Supplementary Material Available: Tables of selected bond distances and angles and structure factor amplitudes (7 pages). Ordering information is given on any current masthead page.

Synthesis and Decay Kinetics of $Ni(CO)_3N_2$ in Liquid Krypton: Approximate Determination of the Ni–N_2 Bond Dissociation Energy

James J. Turner,* Michael B. Simpson, Martyn Poliakoff, and William B. Maier II[1]

Contribution from the Department of Chemistry, University of Nottingham, University Park, Nottingham, England NG7 2RD. *Received October 4, 1982*

Abstract: The unstable species $Ni(CO)_3N_2$ is generated in solution by UV photolysis of $Ni(CO)_4$ in N_2-doped liquid Kr in a specially designed high-pressure cell. We have used IR spectroscopy to follow the subsequent thermal reaction of $Ni(CO)_3N_2$ with dissolved CO to reform $Ni(CO)_4$. The reaction rate has been monitored over the temperature range 112–127 K. The rate shows a first-order dependence on the concentration of $Ni(CO)_3N_2$ and a more complex dependence on the concentrations of CO and N_2. The reaction involves two simultaneous paths, one dissociative and the other probably associative. From the dissociative path, we have estimated the Ni–N_2 bond dissociation energy to be 10 kcal mol^{-1}.

Introduction

Kinetic measurements on unstable inorganic species in solution have been obtained either by "instantaneous" techniques such as flash photolysis[2a] and pulse radiolysis or by pseudo-steady-state methods such as stopped flow.[2b] Unfortunately, these techniques generally provide rather poor structural information about the unstable species. By contrast, matrix isolation can provide excellent structural data about reactive and even highly unstable species, trapped in low-temperature solids,[3,4] but kinetic measurements on these species are generally impossible, except in unusual circumstances.[5] Recently[6] we have used liquefied xenon at −80 °C as a solvent for the photochemical generation of the molecules $Cr(CO)_{6-x}(N_2)_x$, all previously unknown outside low-temperature matrices. The compounds were identified from their IR spectra in specially designed low-temperature/high-pressure cells.[7,8] During this work we also found that the thermal stabilities of the different $Cr(CO)_{6-x}(N_2)_x$ species could be estimated by using a *conventional* IR spectrometer (e.g., for $Cr(CO)_3(N_2)_3$, $t_{1/2} \sim 15$ min at −79 °C).

In this paper, we describe the photochemical generation of a thermally much less stable compound, $Ni(CO)_3N_2$, in liquid krypton. $Ni(CO)_3N_2$ has previously been identified only in low-temperature matrices either by photolysis[9] of $Ni(CO)_4$ in solid N_2 or by co-condensation of Ni atoms with CO/N_2 mixtures.[10] Furthermore, we present quantitative kinetic measurements for the thermal decay reaction

$$Ni(CO)_3N_2 + CO \rightarrow Ni(CO)_4 + N_2$$

over the temperature range 112.5–127 K (which represents a change in kT equivalent to a temperature rise of 40 °C at room temperature).

This type of ligand replacement reaction in substituted metal carbonyl complexes has received considerable attention.[11,12] In particular, tetrahedral nickel (Ni^0, d^{10}) complexes such as $Ni(CO)_4$ obey a single-term rate law in which the ligand substitution process appears to be purely dissociative (D) in character.[13] The bimolecular pathway is predominant,[14-16] however, for the isoelectronic d^{10} species $Co(CO)_3NO$, $Fe(CO)_2(NO)_2$, and $Mn(NO)_3CO$. In the case of the group 6B $M(CO)_5$(amine) compounds the situation is more complicated.

Substitution of amine by a Lewis base such as PR_3 generally follows a two-term rate law:

$$M(CO)_5A + L \rightarrow M(CO)_5L + A$$

whence, in the absence of added free amine (A)

$$k_{obsd} = k_1 + k_2[L] \qquad L = \text{phosphine} \qquad (1)$$

(1) Present address: Los Alamos National Laboratory, Los Alamos, NM 87545.
(2) (a) Bonneau, R.; Kelly, J. M. *J. Am. Chem. Soc.* **1980**, *102*, 1220–1. Geoffroy, G. L.; Wrighton, M. S. "Organometallic Photochemistry"; Academic Press: New York, 1979. (b) Moore, P. *Chimia* **1979**, *33*, 335–7.
(3) Turner, J. J.; Burdett, J. K.; Perutz, R. N.; Poliakoff, M. *Pure Appl. Chem.* **1977**, *49*, 271–85. Moskovits, M.; Ozin, G. A. "Cryochemistry"; Wiley: New York, 1976. Turner, J. J. In "Matrix Isolation Spectroscopy"; Barnes, A. J., et al., Eds.; 1982; pp 495–515.
(4) Burdett, J. K.; Downs, A. J.; Gaskill, G. P.; Graham, M. A.; Turner, J. J.; Turner, R. F. *Inorg. Chem.* **1978**, *17*, 523–32.
(5) Frei, H.; Pimentel, G. C. *J. Phys. Chem.* **1981**, *85*, 3355–60.
(6) Maier, W. B., II; Poliakoff, M.; Simpson, M. B.; Turner, J. J.; *J. Chem. Soc. Chem. Commun.* **1980**, 587–589. Turner, J. J.; Simpson, M. B.; Poliakoff, M.; Maier, W. B., II; Graham, M. A. *Inorg. Chem.* **1983**, *22*, 911.
(7) Maier, W. B., II; Poliakoff, M.; Simpson, M. B.; Turner, J. J. *J. Mol. Struct.* **1982**, *80*, 83–6.
(8) Beattie, W. H.; Maier, W. B., II; Holland, R. F.; Freund, S. M.; Stewart, B. *Proc. SPIE (Laser Spectrosc.)* **1978**, *158*, 113–7.
(9) Rest, A. J. *J. Organomet. Chem.* **1972**, *40*, C76.
(10) Kundig, E. P.; Moskovits, M.; Ozin, G. A. *Can. J. Chem.* **1973**, *51*, 2737–46.
(11) Dobson, G. R. *Acc. Chem. Res.* **1976**, *9*, 300–306. Pardue, J. E.; Dobson, G. R. *Inorg. Chim. Acta* **1976**, *20*, 207–12.
(12) Basolo, F. *Chem. Brit.* **1969**, *5*, 505–10.
(13) Day, J. P.; Basolo, F.; Pearson, R. G. *J. Am. Chem. Soc.* **1968**, *90*, 6927–33.
(14) Thorsteinson, E. M.; Basolo, F. *J. Am. Chem. Soc.* **1966**, *88*, 3929–36.
(15) Morris, D. E.; Basolo, F. *J. Am. Chem. Soc.* **1968**, *90*, 2531–6.
(16) Wawersik, H.; Basolo, F. *J. Am. Chem. Soc.* **1967**, *89*, 4626–30.

0002-7863/83/1505-3898$01.50/0 © 1983 American Chemical Society

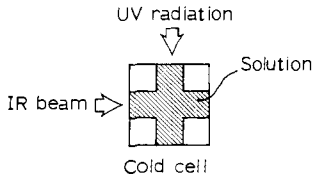

Figure 1. Schematic plan view of the IR cold cell arranged for simultaneous UV photolysis and IR spectroscopy of the liquid-noble-gas solution. The cell is fitted with four spectroscopic windows, one pair (quartz) to transmit UV–vis and the other pair (KRS-5) to pass IR radiation. The IR and UV path lengths are both 2.7 cm, and the cell is equipped with a small magnetic stirrer to ensure rapid mixing of the solution.

This rate law is interpreted in terms of concurrent dissociative and I_D mechanisms.[17]

In the Results, (a) we describe the synthesis of $Ni(CO)_3N_2$ and how the pseudo-first-order rate constant, k_{obsd}, for its reaction with CO was obtained, (b) we show that the dependence of k_{obsd} on the concentrations of free CO and N_2 is only consistent with a rate law (similar to eq 1) involving both dissociative and associative mechanisms (by "associative" we mean any ligand-dependent pathway in which the incoming CO ligand is significantly involved in the transition state), and (c) we use the temperature dependence of k_{obsd} to deduce activation parameters for the two rate constants k_1 and k_2 and find that the apparent activation energy for k_{obsd} is sensitive to CO and N_2 concentrations, because of saturation effects fortuitously arising from the relative values of k_1 and k_2. Finally in the Discussion we assess the relevance of our results to existing thermochemical and kinetic measurements on Ni(0) complexes at room temperature.

Results

(a) Synthesis of $Ni(CO)_3N_2$ and Kinetic Measurements. The species $Ni(CO)_3N_2$ is relatively short lived, even at liquid-krypton temperatures, and in order to observe it successfully one must maintain a steady-state concentration by continuous UV photolysis while the IR spectrum is recorded. In our experiments this was achieved by the use of a four-way liquid cell fitted with opposing pairs of UV and IR spectroscopic windows (Figure 1). Typically our solutions of nickel carbonyl in liquid Kr/N_2 mixtures were in the concentration range $(2.5–5) \times 10^{-4}$ mol dm^{-3}, were optically dense in the UV, and were well mixed by means of a magnetic stirrer and flea. The solutions were prepared by sweeping a measured volume of nickel carbonyl into the cold partially filled cell under krypton pressure. For the kinetic runs, varying quantities of gaseous N_2 doped with CO were dissolved in the krypton solution under pressure.

The IR spectrum of nickel carbonyl dissolved in liquid Kr containing 5% N_2 at 114 K is shown in Figure 2. The broad absorptions centered at approximately 2137 and 2350 cm^{-1} are due to dissolved CO and N_2, respectively. The IR absorption of N_2 is induced by the liquid state. In separate experiments we have shown that both absorptions obey Beer's law and can be used to monitor the concentrations of N_2 and CO. A small concentration of CO is always present in solution due to decomposition of the $Ni(CO)_4$ in the gas manifold, but in the kinetic runs described later, additional CO was deliberately added. The IR bands of $Ni(CO)_4$ (2048 cm^{-1}) and natural abundance $Ni(CO)_3(^{13}CO)$ (2123, 2011 cm^{-1}) are significantly sharper than those of N_2 and CO but also obey Beer's law. The bands are due to $Ni(CO)_4$ authentically in solution, rather than a suspension of solid, and there is no change in the relative band intensities on warming, cooling, or diluting the solution. By contrast, $Ni(CO)_4$ is virtually insoluble in *pure* liquid N_2 at this temperature.

When the stirred solution is irradiated with an unfiltered Cd arc (λ_{max} 229 nm), the bands outlined in a solid line in Figure 3 appear in the IR spectrum recorded simultaneously. The

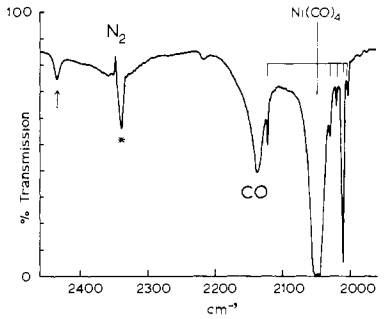

Figure 2. IR spectrum of a solution of $Ni(CO)_4$ (0.5 μmol) in liquefied krypton containing added N_2 and CO ($[N_2]:[CO] = 1500:1$). The path length is 2.7 cm, and the temperature of the solution 112.5 K. The intense absorption at 2050 cm^{-1} is due to $Ni(^{12}CO)_4$, and associated with it are a number of sharp, weaker features due to the naturally occurring ^{13}CO isotopomers of nickel carbonyl. Absorptions due to CO and N_2 show as broad bands centered at approximately 2135 and 2350 cm^{-1}, respectively. The approximate CO concentration is 1.15×10^{-3} M. The band marked with the arrow is the $\nu_5 + \nu_7$ combination band of $Ni(^{12}C-O)_4$. The sharp feature (asterisk) at 2338 cm^{-1} is due to CO_2 present as an impurity at a concentration below 1 ppm.

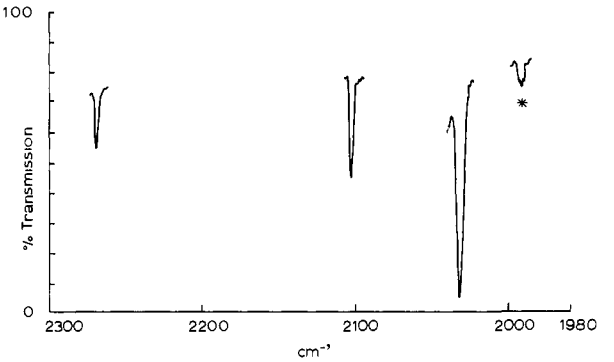

Figure 3. IR spectrum of $Ni(CO)_3N_2$ produced by the UV photolysis of a solution of $Ni(CO)_4$ in liquefied krypton containing 5% N_2 at 114 K. The dashed line represents the spectrum of the solution without photolysis. The solid line indicates absorptions due to $Ni(CO)_3N_2$ that appear in the spectrum while the UV photolysis lamp is on. The band marked with an asterisk is due to natural abundance $Ni(^{12}CO)_2(^{13}CO)N_2$. Band positions are given in Table I. The spectrum was recorded by using a Perkin-Elmer 283B spectrophotometer. The path length was 2.7 cm, and the approximate concentration of $Ni(CO)_3N_2$ is 5×10^{-6} M.

Table I. IR Absorptions (cm^{-1}) of $Ni(CO)_3N_2$

assignment	liquid Kr[a]	solid N_2, 20 K[c]	solid Ar, 10 K[e]
a_1 ν_{N-N}	2267.5 ± 0.5	2266	2264.4
a_1 ν_{C-O}	2101.0 ± 0.5	2098	2100.6
e ν_{C-O}	2030.0 ± 0.5	2031/2027[d]	2029.4
a_1 $\nu_{^{13}C-O}$	1994 ± 1.0[b]		

[a] This work. [b] This band is due to natural abundance $Ni(CO)_2(^{13}CO)N_2$ and may be clearly distinguished at the highest steady-state concentrations of $Ni(CO)_3N_2$. The calculated position of this band based on the $\nu_{^{12}C-O}$ positions and frequency factored force field is 1994.1 cm^{-1}. [c] Reference 9. [d] Matrix splitting. [e] Reference 10.

positions of these absorptions are given in Table I, where they are compared with the known IR absorptions[9,10] of matrix-isolated $Ni(CO)_3N_2$. The species in solution is clearly $Ni(CO)_3N_2$.

The absorptions due to $Ni(CO)_3N_2$ that appear on irradiation of the stirred solution increase in intensity during photolysis and reach a maximum steady-state intensity. When the photolysis lamp is switched off, the bands decrease in intensity but sufficiently slowly for the decay to be monitored with a conventional IR spectrometer operating in the time drive mode (Figure 4). Thus, $Ni(CO)_3N_2$ decays thermally in solution in liquid krypton, and the disappearance of the corresponding IR absorptions may be followed quantitatively.

(17) Covey, W. D.; Brown, T. L. *Inorg. Chem.* **1973**, *12*, 2820–5. Langford, C. H.; Gray, H. B. "Ligand Substitution Processes"; Benjamin: New York, 1965.

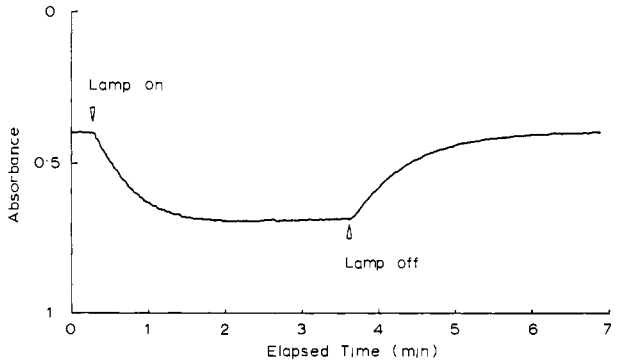

Figure 4. Thermal decay of $Ni(CO)_3N_2$ in liquid krypton/N_2/CO mixture at 119 K. (The CO concentration is 1.07×10^{-3} M, and the ratio $[N_2]$:[CO] is 5000:1.) The decay was monitored by setting the monochromator of a Perkin-Elmer 580A spectrometer at 2030 cm^{-1} (the position of the most intense $Ni(CO)_3N_2$ absorption). The photolysis source was a Cd resonance lamp (λ_{max} 229 nm).

There can be no *direct* spectroscopic evidence that $Ni(CO)_3N_2$ decays thermally to $Ni(CO)_4$, because the maximum steady-state concentration of $Ni(CO)_3N_2$ is ~1.5% of the $Ni(CO)_4$ concentration (i.e., $\sim 7.5 \times 10^{-6}$ M), and any effect on the $Ni(CO)_4$ IR absorptions would be negligible under these conditions. However, there can be little doubt that the reaction is

$$Ni(CO)_3N_2 + CO \rightarrow Ni(CO)_4 + N_2$$

because (a) the decay rate of $Ni(CO)_3N_2$ increases with the amount of free CO in the solution and (b) no overall loss of $Ni(CO)_4$ is observed even after several hours of UV irradiation of a solution containing N_2. On the other hand, irradiation in the *absence* of N_2 leads to the rapid disappearance of $Ni(CO)_4$ and formation of a transient carbonyl species ($t_{1/2} \sim 12$ s at −160 °C; $\bar{\nu}_{C-O}$ 2088, 1908 cm^{-1}, similar to matrix-isolated $Ni_2(CO)_7$[18]) and an unknown precipitate.

Analysis of decay curves such as that in Figure 4 shows that the decay of $Ni(CO)_3N_2$ follows pseudo-first-order kinetics over 3–4 half-lives (eq 2) and the value of k_{obsd} increases substantially

$$-d[Ni(CO)_3N_2]/dt = k_{obsd}[Ni(CO)_3N_2] \quad (2)$$

with temperature from 112.5 to 127 K (Figure 5). At first glance, these results suggest a purely dissociative mechanism, but since we observed a dependence of k_{obsd} on the concentrations of both N_2 and CO, a more careful analysis is required. We need not consider mechanisms in which $Ni(CO)_4$ might be involved in the rate law because we detected no influence on the decay rate over a 2-fold change in $Ni(CO)_4$ concentration. Moreover, we are not observing a diffusion-controlled reaction because the observed rate is at least 10^4 lower than that expected in the diffusion-controlled limit for the concentration of CO present in the solution.

(b) Rate Law for Decomposition of $Ni(CO)_3N_2$. A high concentration of free leaving group (in this case N_2) can affect even a completely dissociative process. This has most recently been noted by Lees and Adamson in flash photolysis studies[19] involving the thermal decay of a loosely complexed $W(CO)_5$···solvent species. The purely dissociative thermal mechanism for the decay of $Ni(CO)_3N_2$ and reformation of $Ni(CO)_4$ involves the steps

$$Ni(CO)_3N_2 \underset{k_{-1}}{\overset{k_1}{\rightleftharpoons}} Ni(CO)_3 + N_2$$

$$Ni(CO)_3 + CO \xrightarrow{k'} Ni(CO)_4$$

whence, by the steady-state approximation and by using the notation of Covey and Brown[17] we obtain the rate law shown in eq 3, where $\gamma = (1 + k_{-1}/k'\cdot[N_2]/[CO])$.

$$k_{obsd} = k_1/(1 + k_{-1}/k'\cdot[N_2]/[CO]) = k_1/\gamma \quad (3)$$

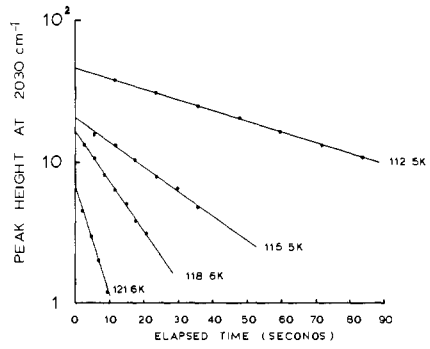

Figure 5. Pseudo-first-order decay of $Ni(CO)_3N_2$ IR absorption at 2030 cm^{-1} (e, ν_{C-O}) at various temperatures in liquid Kr at a fixed concentration of N_2 and CO. The data are obtained directly from thermal decay curves such as Figure 4. The absorbance at 2030 cm^{-1} is taken to be a direct measure of $Ni(CO)_3N_2$ concentration ($\Delta\bar{\nu}_{1/2} = 3$ cm^{-1}, spectral resolution ~2 cm^{-1}). No deviation from linearity was observed over a very large number of such decay plots. The data were fitted by linear regression.

If $[N_2] = 0$, then $k_{obsd} = k_1$ as anticipated. If, however the reaction takes place in the presence of an excess of N_2 (i.e., $[N_2] > 0$), then the observed pseudo-first-order decay rate k_{obsd} will depend on both $[N_2]$ and [CO]. This dependence of k_{obsd} on $[N_2]$ and [CO] is effectively unaltered if the reactive intermediate $Ni(CO)_3$ is solvated, in some preequilibrium step:

$$Ni(CO)_3 \underset{-S}{\overset{S}{\rightleftharpoons}} [Ni(CO)_3\cdot S]$$

The simplest bimolecular pathway is expressed by the step

$$Ni(CO)_3N_2 + CO \xrightarrow{k_2} Ni(CO)_4 + N_2$$

in which case

$$k_{obsd} = k_2[CO] \quad (4)$$

and a direct dependence of the pseudo-first-order rate on [CO] is expected. The same form of dependence of k_{obsd} on [CO] as in eq 4 is expected for an I_d mechanism eq 5, where $k_2' = kK_1$,

$$Ni(CO)_3N_2 + CO \overset{K_1}{\rightleftharpoons} [Ni(CO)_3N_2\cdot CO] \xrightarrow{k} [Ni(CO)_3CO\cdot N_2] \xrightarrow{fast} Ni(CO)_4 + N_2$$

$$k_{obsd} = k_2'[CO] \quad (5)$$

although in this case the rate constant, k_2', is modified by the equilibrium constant, K_1. The derivation of eq 5 and exclusion of $[N_2]$ from the rate law assume that the formation of outer-sphere complexes of the type $[Ni(CO)_3N_2\cdot N_2]$ does not deplete the concentration of free $Ni(CO)_3N_2$ sufficiently to affect the rate law.[20] This assumption seems justified in our experiments, since any outer-sphere complexes formed are at a concentration below the limits of IR detection.

Thus, for a dissociative mechanism, k_{obsd} depends on [CO] and $[N_2]$ while for an associative mechanism k_{obsd} depends on [CO] alone. Since k_{obsd} for $Ni(CO)_3N_2$ depends on both [CO] and $[N_2]$, we must distinguish between a purely dissociative mechanism and a combination of simultaneous dissociative and associative processes, that is, between eq 3 and 6 (where $\gamma = (1 + (k_{-1}/k')\cdot$

$$k_{obsd} = k_1/\gamma \quad (3)$$

$$k_{obsd} = k_1/\gamma + k_2[CO] \quad (6)$$

$([N_2]/[CO])$). The use of premixed gaseous N_2 and CO, which can be condensed into the liquid Kr, allows us to vary [CO] while keeping $[N_2]/[CO]$, and hence γ, constant. Then, a plot of k_{obsd} against [CO] should be linear with slope k_2 and intercept k_1/γ.

Results for two such experiments with $[N_2]/[CO] = 1500$ and 5000 (CO = 0.067% and 0.02%) are shown in Figures 6, A and B, respectively. A linear dependence is observed in both cases

(18) Hulse, J.; Moskovits, M., private communication.
(19) Lees, A. J.; Adamson, A. W. *Inorg. Chem.* **1981**, *20*, 4381–4.
(20) Darensbourg, D. J.; Ewen, J. A. *Inorg. Chem.* **1981**, *20*, 4168–77.

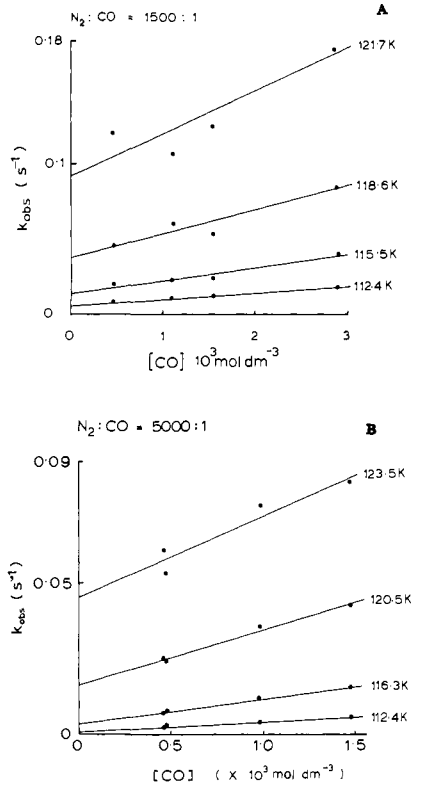

Figure 6. (A) Rate plot of k_{obsd}, the pseudo-first-order decay rate constant of $Ni(CO)_3N_2$, vs. CO concentration at a fixed ratio of $[N_2]$:[CO] 1500:1, at various temperatures. The values of k_{obsd} were determined directly from the pseudo-first-order decay plots such as Figure 5. This plot is designed to detect the presence of concurrent associative (CO-dependent, nonzero slope) and dissociative (N_2:CO-dependent, nonzero intercept) mechanisms. Both slope and intercept were determined by linear regression. (B) As in A except $[N_2]$:[CO] = 5000:1.

Table II

N_2:CO	T, K	$10^2k_1/\gamma$, s^{-1} [a]	10^2k_1, s^{-1} [c]	k_2, dm^3 mol^{-1} s^{-1} [d]
1500	112.5	0.41	2.0	4.1
	115.5	1.2	5.5	8.0
	118.6	3.7	17.6	15.0
	121.6	9.1	43.4	26.0
5000	112.4	(0.035)[b]	(0.47)[b]	3.4
	116.3	0.31	4.2	8.1
	120.5	1.6	21.9	17.7
	123.5	4.5	60.2	27.0

[a] Values of k_1/γ obtained as intercept from plots of k_{obsd} vs. CO at constant ratio $[N_2]$:[CO]; see Figure 6, A and B. [b] Value of intercept at slowest rate subject to significant extrapolation error. [c] Values of k_1 derived from k_1/γ via estimate of γ. A plot of γ/k_1 vs. $[N_2]$/[CO] for $[N_2]$:[CO] equal to 1000, 1500, and 5000 suggests that the competition ratio $k_{-1}/k' \approx 1/400$ whence γ_{5000} = 4.75 and γ_{5000} = 13.5. [d] Calculation of k_2 requires an estimate of the CO concentration. This was obtained in two ways: either by estimation of the volume of N_2:CO mixture condensed into the cell, or from the integrated absorbance of the CO IR absorption at 2135 cm^{-1} and use of available data[30] for the absorption cross section of CO in liquid N_2. The values so obtained agree to within 10%.

with nonzero values for both k_1/γ and k_2. Thus, dissociative and associative (I_A or I_D) mechanisms must be occurring simultaneously.

By allowing the equilibrium pressure over the cell to rise, the decay of $Ni(CO)_3N_2$ may be monitored over a range of temperature (112.4–125 K; $8.9 > 10^3/T > 8.0$), and from Figure 6, A and B, the separate temperature dependencies of k_1/γ and k_2 (intercept and slope, respectively) may be obtained.

(c) Temperature Dependence and Saturation Effects. The values of k_1/γ and k_2 at various temperatures and ratios of $[N_2]$:[CO]

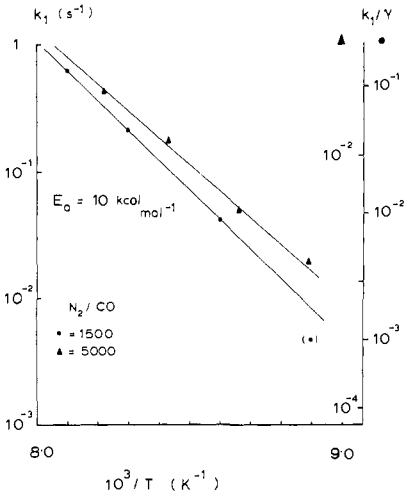

Figure 7. Arrhenius plot for the dissociative rate constant k_1. The right-hand axes gives the numerical values of the intercept, k_1/γ, from Figure 6, A and B, at different temperatures and for two sets of data for two ratios N_2:CO. The data point marked (●) is the lowest measurable value of the intercept and has a large error. The left-hand axis gives the value of k_1 itself corresponding to each data point. The slopes of the lines fitted to the two sets of data differ by less than 1 kcal mol^{-1}; thus, $E_a(k_1)$ is 10 ± 1 kcal mol^{-1}.

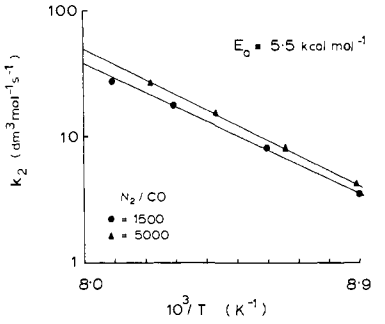

Figure 8. Arrhenius plot for the associative rate constant k_2. The values of k_2 are derived directly from the slopes of Figure 6 A and B. The two sets of data are nearly coincident, and the slopes give a value $E_a(k_2)$ of 5.5 ± 0.5 kcal mol^{-1}.

are given in Table II. The Arrhenius plot for k_1/γ is shown in Figure 7 (right-hand axes) and that for k_2 in Figure 8. These plots give experimental activation energies (E_a) of 10 ± 1 kcal/mol for k_1/γ and 5.5 ± 0.5 kcal/mol for k_2.

The apparent activation energy of k_{obsd} depends critically on the relative contributions of the dissociative (D) and associative (A) processes to the overall rate. These relative contributions in turn depend on $[N_2]$/[CO], and at extreme values of $[N_2]$/[CO] we observe saturation effects with one process dominating to the virtual exclusion of the other. With $[N_2]/[CO] < 1000$, k_1/γ is sufficiently large, compared to k_2[CO], that the decay rate of $Ni(CO)_3N_2$ shows negligible dependence on [CO] over the range available in the experiment and an apparent activation energy of ~9 kcal/mol, almost the same as k_1/γ (Figure 7). Even under these conditions, the associative process should be detectable at high values of [CO], but these lie outside the range possible with our apparatus.

Conversely in experiments with $[N_2]/[CO] \gg 5000$, in the range $100\,000 > [N_2]/[CO] > 10\,000$, we observed a strong dependence of k_{obsd} on [CO] and an experimental activation energy for k_{obsd} of 5.5 kcal mol^{-1}, identical with that of k_2 (Figure 8). Under these circumstances k_1/γ is sufficiently small compared with k_2[CO] that the bimolecular term predominates. Further support for this interpretation is given by the fact that, at a given temperature, the overall observed rate, k_{obsd}, for high values of $[N_2]$/[CO] is *slower* than for smaller $[N_2]$/[CO] ratios.

The Arrhenius plots can provide values of E_a for k_1/γ and k_2, but before discussing the dissociative process in detail, we require

Table III. Rate Constants and Activation Parameters

Dissociative Pathway

reaction	k_1, s^{-1}	$\Delta H_1^{\ddagger}$, kcal mol^{-1}	$\Delta S_1^{\ddagger}$, cal deg^{-1} mol^{-1}	A_1, s^{-1}
$Ni(CO)_3N_2 \xrightarrow{120\ K} Ni(CO)_3 + N_2$ [a]	0.21[c]	10[d]	21.5[e]	2×10^{16} [f]
$Co(CO)_3NO \xrightarrow{300\ K} Co(CO)_2NO + CO$ [b]	5.5×10^{-8}	35	26	1.7×10^{18}

Associative Pathway

reaction	k_2, dm^3 mol^{-1} s^{-1}	$\Delta H_2^{\ddagger}$, kcal mol^{-1}	$\Delta S_2^{\ddagger}$, cal deg^{-1} mol^{-1}	A_2, dm^3 mol^{-1} s^{-1}
$Ni(CO)_3N_2 + CO \xrightarrow{120\ K} Ni(CO)_4 + N_2$	17.0[g]	5.0[h]	−9.2[i]	1.8×10^{11} [j]
$Co(CO)_3NO + PPh_3 \xrightarrow{300\ K} Co(CO)_2PPh_3NO + CO$	1.19×10^{-3}	16.3	−20	8.9×10^{8}

[a] This work, liquid krypton solution. [b] Reference 24, benzene solution. [c] Estimated from k_1/γ values at 119 K by using value of competition ratio from extrapolation of plot of γ/k_1 vs. $[N_2]/[CO]$ to zero $[N_2]/[CO]$. [d] Calculated from temperature dependence of k_1/γ; error ±1 kcal mol^{-1}. [e] Calculated by using estimate of k_1 and value of $\Delta H_1^{\ddagger}$ derived from k_1/γ. If k_1/γ is used directly as rate constant $\Delta S_1^{\ddagger} = +15$ eu, which is a lower limit since $\gamma > 1$. [f] Calculated from $\Delta S_1^{\ddagger}$. [g] See footnote *d* of Table II. [h] Calculated directly from temperature dependence of k_2; error ±0.5 kcal mol^{-1}. [i] Calculated directly from k_2 and $\Delta H_2^{\ddagger}$. [j] Calculated from $\Delta S_2^{\ddagger}$.

an estimate of E_a for k_1 itself and hence an estimate of the magnitude and temperature dependence of γ.

γ is defined as $1 + (k_{-1}/k')([N_2]/[CO])$, where k_{-1} and k' are the rates of reaction of $Ni(CO)_3$ with N_2 and CO, respectively. Both of these addition reactions occur *thermally* in solid matrices annealed to 30 K,[10,21] which implies activation energies below 1 kcal mol^{-1}. Thus, the reaction of $Ni(CO)_3$ with both N_2 and CO may be regarded as effectively activationless[12,22] and γ as independent of temperature over the range of our experiments.

In principle[17] the value of γ may be determined directly from a plot of γ/k_1 vs. $[N_2]/[CO]$ at different temperatures. The values of γ for $[N_2]$:[CO] equal to 1500 and 5000 are given in Table II. Also in Table II are the calculated values of k_1 at various temperatures. Unfortunately, the saturation effects described above limit the usable range of $[N_2]/[CO]$ for this purpose, and the errors involved in extrapolation are large.

Nevertheless the estimates of γ obtained imply that the competition ratio k_{-1}/k' is about 1/400, from which it is estimated that any temperature dependence in k_{-1}/k' cannot lead to a contribution to the activation energy $E_a(k_1/\gamma)$ much greater than 1.0 kcal mol^{-1}. This suggests that within experimental error, $E_a(k_1/\gamma) = E_a(k_1)$. The Arrhenius plots in Figure 7, therefore, apply equally for k_1 and k_1/γ and are thus relabeled for k_1 on the left-hand axis. The near coincidence of the two sets of data suggests that our estimates of γ are reasonable.

Having now established the experimental activation energies (E_a) for both k_1 and k_2 separately, it is possible to evaluate the thermodynamic quantities[23] $\Delta H_1^{\ddagger}$, $\Delta S_1^{\ddagger}$ $\Delta H_2^{\ddagger}$, and $\Delta S_2^{\ddagger}$, (the subscripts 1 and 2 refer respectively to the dissociative and associative activation pathways). Calculation of $\Delta S_1^{\ddagger}$ requires a knowledge of the *absolute* value of k_1, which in turn requires the value of γ.

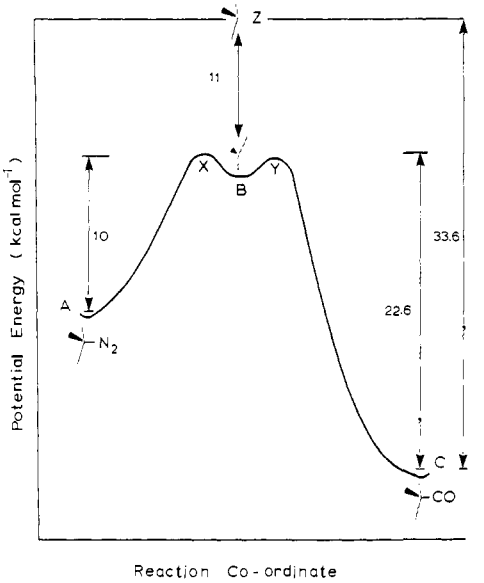

Figure 9. Reaction profile for the unimolecular decomposition of $Ni(CO)_3N_2$: A = $Ni(CO)_3N_2$; B = $Ni(CO)_3[D_{3h}]$; C = $Ni(CO)_4$; Z = $Ni(CO)_3[C_{3v}]$. $\Delta E_{AX}^{\ddagger}$ and $\Delta E_{CY}^{\ddagger}$ are experimentally determined activation parameters; ΔE_{CZ} and ΔE_{BZ} are theoretically calculated energy values. See text for discussion. The figure shows that in the transition state the activated complex, either $Ni(CO)_3 \cdots N_2$ or $Ni(CO)_3 \cdots CO$ has substantially relaxed toward the D_{3h} geometry and about 11 kcal mol^{-1} is saved by this process. Consequently the activation barriers for reaction of D_{3h} $Ni(CO)_3$ with CO or N_2 are slight.

However, we can obtain a *lower limit* for the value of $\Delta S^{\ddagger}$ without using γ. Equation 3 shows that $\gamma > 1$ under all circumstances, since $[N_2] > [CO]$. Therefore, the values of the intercepts in Figure 6, actually k_1/γ, must be lower than the values of k_1 itself. Thus, the value of $\Delta S_1^{\ddagger}$ derived from these intercepts is a lower limit. The value so obtained in +15 cal deg^{-1} mol^{-1}. The value of $\Delta S_1^{\ddagger}$ obtained by using the best estimate of k_1 itself is +21.5 cal deg^{-1} mol^{-1}. $\Delta S_2^{\ddagger}$ can be calculated directly from Figure 8. All these activation parameters are collected in Table III.

The approximate values of $\Delta S_1^{\ddagger}$ and $\Delta S_2^{\ddagger}$ in Table III are consistent with known values for dissociative and associative processes in tetrahedral d^{10} complexes.[24]

(21) DeKock, R. L. *Inorg. Chem.* **1971**, *10*, 1205–11.

(22) Basolo has suggested that for $Ni(CO)_3 + CO \rightarrow Ni(CO)_4$, $\Delta H^{\ddagger} \simeq 9.7$ kcal mol^{-1} and $\Delta S^{\ddagger} = -27$ eu. This is surely inconsistent with the matrix results and the data in this paper; see also the Discussion.[12]

(23) In the *condensed phase* the thermodynamic parameters $\Delta H^{\ddagger}$ and $\Delta S^{\ddagger}$ are defined in transition-state theory by

$$k = k_B T/h \exp(\Delta S^{\ddagger}/R) \exp(-\Delta H^{\ddagger}/RT)$$

(k_B = Boltzman constant). The activation energy, E_a, is defined by the Arrhenius equation

$$E_a = RT^2 \, d \ln k/dT$$

whence $\Delta H^{\ddagger} = E_a - RT$ and $\Delta S^{\ddagger} = R \ln Ah/ek_BT$. The statistical mechanical formulation gives

$$k = \frac{k_B T}{h} \frac{Q^{\ddagger}}{Q} \exp(\Delta E_0^{\ddagger}/RT)$$

where $\Delta E_0^{\ddagger}$ is the energy difference between reactant and activated complex, whence $E_a = \Delta E_0^{\ddagger} + RT$ (7).

(24) Cardaci, G.; Foffani, A.; Distefano, G.; Innorta, G.; *Inorg. Chim. Acta.* **1962**, *1*, 340–6.

The values obtained for the thermodynamic parameters in liquid krypton are likely to be closely related to those in the gas phase, and their significance is discussed below.

Discussion

(1) Energetics. The comparison between experimental activation energy and molecular bond energies is best achieved by casting the transition-state theory in a statistical mechanical form, from which eq 7 may be derived.[23] At 150 K, E_a is very nearly

$$E_a = \Delta E_0^{\ddagger} + RT \quad (7)$$

equal to $\Delta E_0^{\ddagger}$, the potential-energy difference between reactants and activated complex. Thus, Figure 9 shows what we believe is a reliable energy profile for the dissociative reaction between $Ni(CO)_3N_2$ and CO.

In Figure 9, the point B represents a planar $Ni(CO)_3$ intermediate with D_{3h} symmetry; this is the known ground-state geometry, from matrix-isolation experiments.[21] As mentioned above, the energy path from $Ni(CO)_3$ to either $Ni(CO)_3N_2$ (A) or $Ni(CO)_4$ (C) involves very low barriers via X and Y, where these are presumably species with weak Ni–N_2 and weak Ni–CO interactions, respectively. (In Figure 9, X and Y have for convenience been given the same energy value, although the kinetic data suggest that $Ni(CO)_3$ discriminates between incoming N_2 and CO groups.) The energy barriers $\Delta E_{AX}^{\ddagger}$ and $\Delta E_{CY}^{\ddagger}$ can, within experimental error, be equated to the E_a values for the respective dissociative reactions of $Ni(CO)_3N_2$ (this work) and $Ni(CO)_4$.[13,25] Thus, assuming that $\Delta E_{BX}^{\ddagger}$ and $\Delta E_{BY}^{\ddagger}$ can be ignored, $\Delta E_{AB} = \Delta E_{AX}^{\ddagger}$ and represents the bond dissociation energy, D_1, of $Ni(CO)_3N_2$. Also $\Delta E_{CB} = \Delta E_{CY}^{\ddagger}$ and represents the corresponding energy, D_2, for $Ni(CO)_4$:

$$Ni(CO)_3N_2 \rightarrow Ni(CO)_3[D_{3h}] + N_2 \qquad D_1 \sim 10 \text{ kcal mol}^{-1}$$

$$Ni(CO)_4 \rightarrow Ni(CO)_3[D_{3h}] + CO \qquad D_2 \sim 23 \text{ kcal mol}^{-1}$$

Recent theoretical calculations[26] lead to a value for D_2 of 22.5 kcal mol^{-1}, which is only 0.5 kcal mol^{-1} less than the experimental value of $\Delta E_{CY}^{\ddagger}$. This provides further evidence that $\Delta E_{BY}^{\ddagger}$ (and hence $\Delta E_{BX}^{\ddagger}$) must be small and hence that the activation energy for the $Ni(CO)_3N_2$ reaction should be a good estimate of D_1.

Independent evidence for the value of D_2 is now available through laser photoelectron spectroscopy,[31] and the value obtained is 25 ± 2 kcal mol^{-1}. The values for D_2 of 23–25 kcal mol are different from the mean thermochemical Ni–CO bond energy[27] in $Ni(CO)_4$ (35.2 kcal mol^{-1}), which merely represents an average over successive ligand dissociation steps.[28] This good agreement between kinetic, theoretical, and experimental methods in the case of $Ni(CO)_4$ encourages us to believe that the kinetically determined value of D_1 in this case (10 kcal mol^{-1}) is a good estimate for the Ni–N_2 bond dissociation energy in $Ni(CO)_3N_2$.

The extended Hückel calculations cited above also suggest an energy difference for

$$Ni(CO)_3[D_{3h}] \rightarrow Ni(CO)_3[C_{3v}]$$

of 11 kcal mol^{-1}. The low Ni–N_2 bond dissociation energy in $Ni(CO)_3N_2$ is partly due to the fact that this relaxation energy is saved during the dissociation step when the $Ni(CO)_3$ fragment relaxes to D_{3h} symmetry.

Thus, our kinetic experiments on $Ni(CO)_3N_2$ can be combined with previous experiments on $Ni(CO)_4$ and with theoretical work to provide the first energetic data for the Ni–N_2 bond.

All these data are summarized in Table IV.

Table IV. Experimental and Calculated Bond Energies in $Ni(CO)_3N_2$ and $Ni(CO)_4$

process	ΔE (kcal mol^{-1})
$Ni(CO)_4 \rightarrow Ni(CO)_3[D_{3h}] + CO$	23[a]
$Ni(CO)_4 \rightarrow Ni(CO)_3[C_{3v}] + CO$	33.6[b]
$Ni(CO)_3N_2 \rightarrow Ni(CO)_3[D_{3h}] + N_2$	10[c]
$Ni(CO)_3N_2 \rightarrow Ni(CO)_3[C_{3v}] + N_2$	21[d]

[a] Experimental values[12,13] for activation energy lie between 22 and 24 kcal mol^{-1}. [b] Calculated energy difference.[26] [c] This work. [d] This work plus calculated relaxation energy.[26]

(2) Mechanism. In mechanistic terms there may not be that much difference between the "dissociative" and "associative" pathways. If the $Ni(CO)_3$ fragment in the first pathway becomes solvated with Kr, this solvation and the departure of the N_2 ligand may well be concerted, so to some extent, the "dissociative" process could be bimolecular. What marks the difference between the two processes are the relative energies involved. Solvation by Kr hardly affects the energy required to remove the N_2 ligand[29] and has no affect on the rate equation. Attack by CO significantly lowers the activation barrier and reveals itself by an appearance in the rate law:

$$k_{obsd} = k_1/\gamma + k_2[CO]$$

The occurrence of both ligand-dependent and dissociative pathways with about the same rate at 120 K shows that the *free-energy* barrier to activation in each case is about the same, although $\Delta H_1^{\ddagger} \approx 2\Delta H_2^{\ddagger}$ because of the respectively negative and positive $-T\Delta S$ term.

The k_2 pathway may be understood as either an I_A or I_D process. Any distinction between these in this case can only be made on the basis of the relative activation enthalpies for the dissociative and ligand-dependant pathways. Since $\Delta H_1 \approx 2\Delta H_2$, it appears that the incoming CO ligand has significant energetic involvement in the transition state, and the ligand-dependant pathway is perhaps best described as an I_A process.

At first sight, the two-term rate law seems markedly different from the observed kinetic behavior of $Ni(CO)_4$ in room-temperature ligand substitution reactions, which appear to follow simple dissociative pathways,[13] and more in line with the behavior of the isoelectronic carbonyl/nitrosyl compounds[14,15] $Fe(CO)_2(NO)_2$ and $Co(CO)_3(NO)$. However, if two alternative reaction pathways with differing activation parameters are available, then the relative dominance of one pathway over another is critically influenced by temperature. This effect has previously been noticed, for example, in the reactions of $Co(CO)_3NO$, where[24] between 27 and 46.4 °C the ratio of dissociative to associative rate constants in the reaction of $Co(CO)_3NO$ with PPh_3 in benzene changes by 2 orders of magnitude.

The parameters in Table III, allow us to estimate the effect of temperature on the reaction pathways in $Ni(CO)_3N_2$. The results are shown in Figure 10, which indicates that the ratio k_1/k_2 would change by *5 orders of magnitude* between 120 and 290 K. At the higher temperature, the *dissociative* process completely dominates. Similarly, by assuming an associative pathway for the ligand substitution process in $Ni(CO)_4$, which at room temperature and low entering ligand concentration is simply too low to detect (say $k_1:k_2 = 10^3:1$ and $\Delta H_1^{\ddagger} > \Delta H_2^{\ddagger}$ by about 5 kcal mol^{-1}, as in $Ni(CO)_3N_2$), then if the reaction temperature is reduced to 120 K the associative pathway becomes predominant (albeit vanishingly slow!).

The fact that the choice of reaction pathway is largely predetermined by the temperature of measurement is general and is of particular significance for series of compounds with widely varying stability. For relatively stable compounds there may be no alternative to measuring reaction kinetics at room temperature, since at reduced temperature the rates may be immeasurably slow. For unstable complexes, there is a choice of using "instantaneous" techniques at room temperature or pseudo-steady-state methods

(25) Day, J. P.; Pearson, R. G.; Basolo, F. *J. Am. Chem. Soc.* **1978**, *90*, 6933–38.
(26) McKinney, R. J.; Pensak, D. A. *Inorg. Chem.* **1979**, *18*, 3413–7.
(27) Cotton, F. A.; Fischer, A. K.; Wilkinson, G. *J. Am. Chem. Soc.* **1959**, *81*, 800–3.
(28) Smith, G. P.; Laine, R. M. *J. Phys. Chem.* **1981**, *85*, 1620–2.
(29) Rossi, A.; Kochanski, E.; Veillard, A. *Chem. Phys. Lett.* **1979**, *66*, 13–5.
(30) Brueck, S. R. J.; Osgood, R. M., Jr. *Chem. Phys. Lett.* **1976**, *39*, 568–72.
(31) Stevens, A. E.; Feigerle, C. S.; Lineberger, W. C. *J. Am. Chem. Soc.* **1982**, *104*, 5026–31.

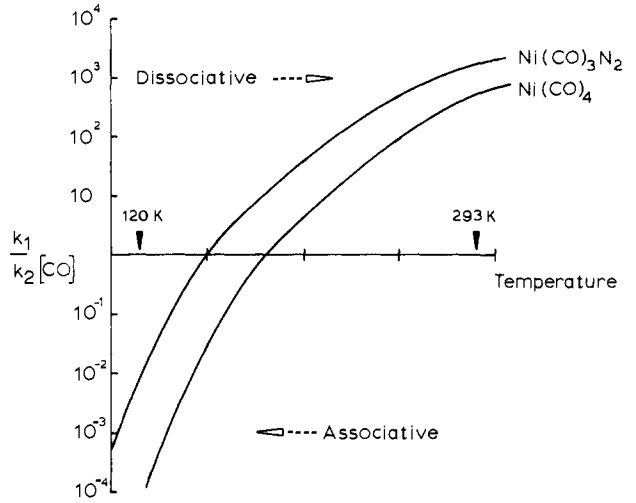

Figure 10. Temperature dependence of mechanisms. The curves have been calculated by using, for $Ni(CO)_3N_2$, experimentally determined activation parameters for the dissociative and associative pathways and, for $Ni(CO)_4$, experimental values for the dissociative mechanism and estimated parameters for an associative pathway similar to $Ni(CO)_3N_2$ but assuming that at 298 K, $k_1/k_2 \simeq 10^3$, i.e., the associative mechanism lies below the limit of observation at moderate entering ligand concentrations. The figure shows that the observed ratio k_1/k_2 and therefore the contribution of an associative pathway to the total rate depend strongly upon the temperature of measurement. The calculation of the rate of the associative pathway in each case assumes [CO] = 1 mol dm^{-3}.

such as we have described here at low temperatures. It is clear from our experiments that results obtained at widely different temperatures will not necessarily be equivalent.

Conclusion

In this paper we have described experiments that demonstrate the existence of the unstable species $Ni(CO)_3N_2$ in solution. Kinetic measurements show that this species decays thermally by reaction with CO, following a two-term rate law best interpreted as being due to a 2-fold reaction pathway involving both a D and an I_A process. Although the precise molecular mechanisms for these processes cannot be determined uniquely from these experiments alone, activation parameters have been obtained, and in the case of the dissociative pathway this allows us to estimate the Ni–N_2 bond dissociation energy in the complex as 10 ± 1 kcal mol^{-1}. We are optimistic that the liquefied noble-gas technique will be helpful in obtaining further information about the reactivity in solution of other unstable species.

Experimental Section

The magnetically stirred IR cold cell, the liquid-nitrogen cooling system, and the gas handling system have been described in detail elsewhere.[7,8] Of particular relevance to the present experiments is the temperature controller, which maintains the temperature of the cell ±0.25 K by a feedback device and iron/constantan thermocouple. The thermocouple was calibrated by measuring the freezing point, −157.3 °C, of a small volume of pure krypton condensed in the cell. (Note that Kr/N_2 mixtures have a significantly lower freezing point than pure Kr.)

The cell was filled by condensing a small volume of krypton (Matheson research grade and BOC research grade 99.9995% purity) into the cooled cell under pressure. A known pressure of degassed $Ni(CO)_4$ (measured with an Appleby–Ireland multitron gauge with digital readout accurate to 0.1 mbar) was trapped within a known volume of the stainless steel gas manifold, previously passivated with 50 mbar of $Ni(CO)_4$. This measured quantity of nickel carbonyl was then swept into the cold, stirred cell under a pressure of krypton and the cell allowed to fill. Finally, N_2 and CO (BOC research grade, accurately premixed by the supplier in aluminium cylinders) were added with vigorous stirring. The concentrations of CO and N_2 were estimated from the manually integrated areas of their IR absorptions (Figure 1), both of which were shown to obey Beer's law under the conditions of our experiments.

The cold cell was set up in the sample compartment of an IR spectrometer for simultaneous IR spectroscopy and UV photolysis (Philips 25-W Cd arc). Survey spectra were run on a Perkin-Elmer Model 283B spectrometer. Kinetic measurements were made on a Perkin-Elmer 580A ratio recording spectrometer set in the time drive mode at 2030 cm^{-1}, the position of the most intense ν_{C-O} band of $Ni(CO)_3N_2$.

Acknowledgment. We thank the SERC for support and for a Senior Visiting Fellowship (to W.B.M.). We are also grateful to Professor J.A. Connor for discussions on bond energies.

Registry No. $Ni(CO)_3N_2$, 37936-21-3; N_2, 7727-37-9; CO, 630-08-0; Ni, 7440-02-0; $Ni(CO)_4$, 13463-39-3.